Title
Principles of X-ray Magnetic Dichroism Spectro-Microscopy

Author
Stohr, J.

Publication Date
1998-06-23

LBNL-41989
LSBL-469
Preprint

ERNEST ORLANDO LAWRENCE
BERKELEY NATIONAL LABORATORY

Principles of X-Ray Magnetic Dichroism Spectro-Microscopy

J. Stöhr, S. Anders, and T. Stammler

Advanced Light Source Division

June 1998

Submitted to
Surface Review and Letters

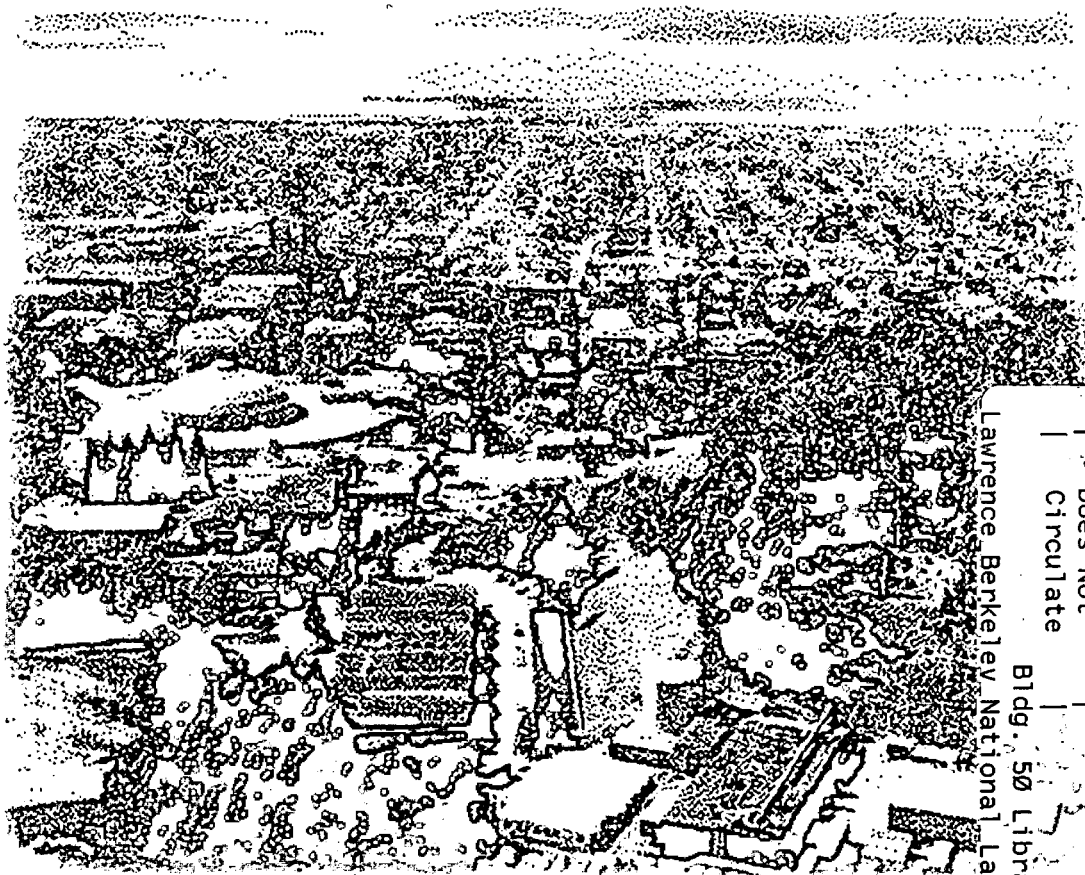

DISCLAIMER

LBNL-41989
LSBL-469

Principles of X-Ray Magnetic Dichroism Spectro-Microscopy

J. Stöhr

IBM Research Division
Almaden Research Center
650 Harry Road
San Jose, CA 95120

S. Anders and T. Stammler

Advanced Light Source Division
Ernest Orlando Lawrence Berkeley National Laboratory
University of California
Berkeley, CA 94720

June 1998

This work was supported by the Laboratory Technology Research Partnership Program, Office of Energy Research, U.S. Department of Energy under a CRADA (Cooperative Research and Development Agreement) between Lawrence Berkeley National Laboratory and IBM, Almaden, and by the Office of Energy Research, Office of Basic Energy Sciences, of the U.S. Department of Energy under Contract No. DE-AC03-76SF00098.

To be published in "Surface Review and Letters" 1998

Principles of X-Ray Magnetic Dichroism Spectro-Microscopy

J. Stöhr
IBM Research Division, Almaden Research Center, 650 Harry Road, San Jose, CA 95120

S. Anders, T. Stammler
Advanced Light Source, Lawrence Berkeley National Laboratory, 1 Cyclotron Road, Berkeley, CA 94720

A review is given of the principles underlying x-ray magnetic circular (XMCD) and linear (XMLD) dichroism spectro-microscopies consisting of polarized x-ray absorption spectroscopy in conjunction with scanning or imaging microscopy. The techniques are shown to have many useful and important capabilities for the study of complex magnetic materials. They offer elemental specificity, chemical specificity, and variable depth sensitivity, among others. XMCD microscopy is best suited for the study of ferromagnets and ferrimagnets and it allows a quantitative determination of the size and direction of spin and orbital moments. XMLD microscopy promises to become a powerful tool for the study of antiferromagnets which are difficult to study by conventional microscopy techniques.

I. INTRODUCTION

The ability to control thin film growth at the atomic level has led to a renaissance in research in magnetism and magnetic materials during the last decade. The renaissance is partly driven by the interesting physics of these complex, often layered, materials and it is clearly fueled by the $50 billion dollar per year magnetic storage industry. As illustrated in Figure 1 structures containing artificially layered magnetic and non-magnetic thin films are the foundation of magnetic recording heads and disks used in todays computers [1]. Ever increasing storage needs drive the miniaturization of all components, in particular the size of the recording heads and the size of the stored bits on the disk. Magnetic storage technology is predicted to continue its domination in the next decade or so. Magnetic materials may even have applications in computer memory, the holy grail of semiconductor devices. Magnetic memory cells, where the 1 and 0 bits correspond to different orientations of non-volatile magnetic domains [2,3], post a challenge to conventional dynamic random access memory (DRAM) and may well be used in tomorrows computers. The extensive use of hard and soft magnets in electric power production and utilization also contributes to the motivation for research into new magnetic materials.

Advances in growth of increasingly sophisticated and interesting magnetic nanostructures require advances in experimental probes that are sensitive to the compositional and magnetic microstructure. Desired capabilities are elemental, chemical and structural sensitivities over a wide range of spatial dimensions, lateral and depth, coupled with a sensitivity to the size and orientation of the magnetic moments. XMCD spectro-microscopy, first demonstrated in 1993 [4,5], offers many of these capabilities. XMLD spectro-microscopy has not been demonstrated to date but from our present understanding [6–10] it is safe to predict that this technique will offer many exciting opportunities in the future. Here we discuss the principles underlying the two techniques. Particular emphasis is given to the microscopy method that is most closely related to low energy electron microscopy (LEEM), namely x-ray photoelectron emission microscopy (X-PEEM). This technique combines secondary electron imaging with scanning of the photon energy to obtain spectroscopic contrast.

II. PRINCIPLES OF XMCD AND XMLD SPECTROSCOPY

Spectro-microscopy combines the principles of spectroscopy with those of microscopy [11]. In this Section we shall review the spectroscopy aspects.

Some of the most powerful spectroscopy methods are based on the absorption of photons since this process is guided by simple electronic dipole transitions. X-rays offer the advantage over visible light that the spectroscopy becomes element specific. The elemental specificity arises from the characteristic binding energies of the atomic core electrons as illustrated in Figure 2a. X- ray absorption (XAS)and x-ray photoelectron spectroscopy (XPS) are the two most widely used core electron spectroscopies. In the following we shall only discuss XAS and its application for microscopy. The choice of XAS over XPS is based on several reasons. XAS is the simpler technique in terms of instrumentation, it is less demanding with respect to photon flux and, most importantly, it can probe samples in a bulk sensitive (transmission) or surface sensitive (electron yield detection) mode, which is of great importance for artificially made multilayer structures. The x-ray absorption spectrum directly exhibits the characteristic absorption edges of the elements in the sample, as shown in Fig. 2b for a $Tb_{24.5}Fe_{70.5}Co_{5.0}$ alloy. At the absorption thresholds of the elements the spectrum shows strong resonances arising from transitions to unfilled valence band states. Since the transitions are governed by the $\Delta l = \pm 1$ selection rule, the d band transition metals are best studied using $L_{2,3}$-edges ($2p \rightarrow d$) and the rare earths using $M_{4,5}$-edges ($3d \rightarrow 4f$), as shown

in Figure 2b for Fe and Co ($L_{2,3}$-edges) and Tb ($M_{4,5}$-edges). X-ray absorption spectroscopy is also sensitive to the chemical environment, similar to XPS, as shown in Figure 2c, where the fine structure of the L_3-edge of an oxidized Fe film is shown.

In practise, x-ray absorption spectroscopy is carried out with polarized synchrotron radiation. Use of the x-ray polarization enables studies of the electronic and magnetic anisotropies of a sample. The polarization characteristics of synchrotron radiation from a bending magnet source are illustrated in Figure 3. If the beam line only accepts radiation through a horizontal slit positioned in the plane of the electron storage ring the x-rays are linearly polarized as shown in red on the right side of the figure. Linear polarized light can be described by a biaxial electric field vector. If, instead the horizontal aperture is placed below the orbit plane of the ring the electrons in the ring appear to rotate counterclockwise and the resulting electron angular momentum is transferred to the emitted photon, as shown in the middle panel of Figure 3. The transmitted radiation is right circularly polarized. For right circularly polarized (RCP) photons the electric field vector $\vec{E}$ of the x-rays rotates counterclockwise about the x-ray emission direction $\vec{k}$ if viewed toward the source and clockwise if viewed in the direction of $\vec{k}$. RCP photons carry an angular momentum $+\hbar$ and can be characterized by a vector, the photon spin, which by definition is in the direction of $\vec{k}$ [12]. The opposite senses of electron and electric field vector rotations apply for an aperture placed above the plane of the storage ring, as shown on the left side of Figure 3, and left circularly polarized (LCP) photons are obtained in this case.

The simple description of the photon polarization by a biaxial vector for linear polarization and a vector for handed circular polarization is the physical basis for probing various anisotropies of the sample. In general, linearly polarized light can only detect an anisotropy of the electronic charge, i.e. its quadruple moment which is related to the square of the electron angular momentum. In contrast, handed circularly polarized light can measure a dipolar or vector quantity, in our case the size and direction of the electron angular momentum and spin.

A. XMCD Spectroscopy

The concepts of XMCD spectroscopy are illustrated in Figure 4 for a d transition metal. Here we have assumed that the d shell has a spin moment which is given by the imbalance of spin-up and spin-down electrons (states below the Fermi level, denoted E_F) or equivalently (except for a change of sign) by the imbalance of spin-up and spin-down holes (states above the Fermi level). In order to measure the difference in the number of d holes with up and down spin, we need to make the x-ray absorption process spin dependent. This is done by use of right or left circularly polarized photons which transfer their angular momentum, $+\hbar$ and $-\hbar$, respectively, to the excited photoelectron. The photoelectron carries the transferred angular momentum as a spin or an angular momentum, or both [13]. If the photoelectron originates from a spin-orbit split level, e.g. the $p_{3/2}$ level (L_3 edge), the angular momentum of the photon can be transferred in part to the spin through the spin-orbit coupling. RCP photons transfer the opposite momentum to the electron than LCP photons, and hence photoelectrons with opposite spins are created in the two cases. Since the $p_{3/2}$ (L_3) and $p_{1/2}$ (L_2) levels have opposite spin-orbit coupling ($l+s$ and $l-s$, respectively) the spin polarization will be opposite at the two edges. In the absorption process, "spin-up" and "spin-down" are defined relative to the photon helicity or photon spin. Since spin flips are forbidden in electric dipole transitions governing x-ray absorption, spin-up (spin-down) photoelectrons from the p core shell can only be excited into spin-up (spin-down) d hole states. Hence the spin-split valence shell acts as a detector for the spin of the excited photoelectron and the transition intensity is simply proportional to the number of empty d states of a given spin.

The quantization axis of the valence shell "detector" is given by the magnetization direction. The size of the dichroism effect scales like $\cos\theta$, where θ is the angle between the photon spin and the magnetization direction. Hence the maximum dichroism effect (typically 20%) is observed if the photon spin direction and the magnetization directions are parallel and antiparallel as shown on the right side of Figure 4. When the photon spin and the magnetization directions are perpendicular the resonance intensities at the L_3 and L_2 edges lie between those obtained for parallel and antiparallel alignments.

The differences in the intensities at the L_3 and L_2 edges for parallel and antiparallel orientation of photon spin and magnetization directions are quantitatively related by sum rules to the size of the spin and orbital magnetic moments [14,15] and to the anisotropies of the spin density and orbital moment [16]. XMCD spectroscopy can therefore determine the sizes, the directions, and anisotropies (sizes in different directions) of the atomic magnetic moments.

B. XMLD Spectroscopy

It is well known that linear polarized x-rays can probe the orientation of molecular orbitals. This is one of the strengths of near edge x-ray absorption fine structure, NEXAFS, spectroscopy [17]. More generally, polarized x-ray absorption can sense the charge anisotropy of the valence states involved in the core excitation process [18,19]. The electric field vector $\vec{E}$ of the linearly polarized x-rays acts as a search light for the number of valence holes in different directions of the atomic volume or the Wigner-Seitz cell. In most cases the anisotropy of the

charge in the atomic volume is caused by an anisotropy in the bonding, i.e. by the electrostatic potential.

A less known effect, which is the basis of XMLD spectroscopy, arises from the presence of a magnetic anisotropy in the sample [6–10]. Let us consider the case of NiO. Because of the cubic symmetry of the lattice the charge distribution around the atoms is nearly spherical and no linear dichroism effect exists in the absence of magnetic interactions. NiO is antiferromagnetic, however, and the Ni spins are oriented in the $(1,1,1)$ plane along the $[\bar{2},1,1]$ axis in the fcc lattice [20]. There is no net magnetic moment because an equal number of spins point into opposite directions, so only a preferential magnetic axis exists. The alignment of the local atomic spins along this axis breaks the cubic symmetry of the charge through the spin orbit coupling. As a consequence the charge exhibits a small anisotropy in the unit cell, i.e. it is no longer spherical but shows an ellipse-like distortion about the magnetic direction. This charge anisotropy leads to an asymmetry of the x-ray absorption signal through the search light effect. The maximum XMLD effect is obtained for $\vec{E}$ parallel versus $\vec{E}$ perpendicular to the magnetic axis. In contrast to the XMCD effect the XMLD effect has a $\cos^2\theta$ dependence, where θ is the angle between $\vec{E}$ and the magnetic axis. In general, the XMLD effect is small in $3d$ metals owing to the small size of the spin orbit interaction and the large band width, resulting in a small charge anisotropy when the d states are summed over the Brillouin zone. However, a sizeable XMLD effect (of order 10%) may be observed in the presence of multiplet splitting. Multiplet finestructure in the L_3 and L_2 resonances is typically observed in transition metal compounds [21] as shown in Fig. 5 for the x-ray absorption spectrum of NiO. At a particular multiplet energy only selected d valence states are probed through matrix element effects that enhance the XMLD effect. In Fig. 5 the XMLD effect is especially visible at the Ni L_2-edge where a sizeable difference is observed for $\vec{E}$ parallel (green) versus perpendicular (red) to the magnetic axis.

III. PRINCIPLES OF XMCD AND XMLD MICROSCOPY

The two basic requirements for microscopy are spatial resolution and contrast. Similar to electron microscopy one can use scanning or imaging methods to obtain spatial resolution as illustrated in Figure 6. In the following we shall discuss these two approaches first and then we consider the various contrast mechanisms.

A. Scanning X-Ray Microscopy

In scanning x-ray microscopy the x-ray beam is focussed to the smallest possible spot size and the x-ray intensity transmitted through the sample, or the fluorescent x-ray or electron intensity from the sample is monitored as a function of the focussed beam position on the sample (either the sample of the beam position may be scanned) [22]. In this approach the spatial resolution is determined by the size of the x-ray spot. Small x-ray spots can be obtained by using the reflected and focussed beam from grazing incidence mirrors or the diffracted and focussed beam from a multilayer mirror or a zone plate. In practise, zone plate focussing, shown in Figure 6 is yielding the smallest spot sizes. The focal spot size is determined by the width of the outermost zones of the zone plate [23] and todate resolutions of 24nm have been obtained [24] with expected resolutions near 20nm in the future. Because the focal length of the zone plate lens changes with photon energy the sample position also needs to be scannable along the beam direction. X-ray transmission or fluorescent microscopy is well suited for studies in the presence of a magnetic field, contrary to electron based methods, and it is bulk sensitive as discussed below.

B. X-ray Photoelectron Microscopy

The second x-ray microscopy method is based on electron detection, only, and was pioneered by Tonner [25]. Because of the close relationship of PEEM and LEEM we shall discuss the principles of PEEM microscopy in more detail. The sample is illuminated by an x-ray beam that is only moderately focussed, e.g. to tens of micrometers, so that it matches the maximum field of view of a photoelectron microscope. The lateral resolution is determined by the electron optics in the PEEM and is limited by three quantities: spherical aberration, chromatic aberration and diffraction. In practise, for x-ray excitation of electrons chromatic aberrations dominate [25,26]. They originate from errors in the focussing of electrons with different kinetic energies.

Most PEEM microscopes do not incorporate an energy analyzer or filter [27] and the detected electrons are mostly low energy secondary electrons as illustrated in Figure 7. X-ray excitation produces photoelectrons with a characteristic energy distribution. The electron intensity is dominated, by orders of magnitude, by the secondary electron tail in the 0-20eV kinetic energy range, where zero kinetic energy corresponds to the vacuum level of the sample [28]. The secondary electron signal, which closely follows the x-ray absorption spectrum of the sample [28], determines the X-PEEM intensity and resolution. Its large intensity provides a suitably large PEEM signal but the energy spread of the inelastic tail (about 5eV for most materials [29]) spoils the resolution through chromatic aberrations.

Fortunately, the effective width of the energy spread is reduced by a suitable aperture placed in the backfocal plane of the PEEM, as shown in Figure 6. The aper-

ture acts as a filter for high energy electrons which are focussed behind the aperture while the low energy portion of the inelastic tail is properly focussed at the aperture position and is thus transmitted. The transmitted portion is schematically shown in red in Figure 7. Calculations show that a spatial resolution in the 10-20nm range can be obtained by X-PEEM because of the energy filtering effect of the aperture [30]. Even better spatial resolutions are achieved when the energy spread of the emitted electrons is reduced. This situation is encountered when ultraviolet radiation is used with an energy slightly higher than the workfunction and a spatial resolution of 8nm has been demonstrated [31]. In this case chromatic aberrations are strongly reduced by the narrow width of the secondary electron distribution. At x-ray energies 22nm have been achieved by use of an energy filter to reduce the electron energy spread [32]. In the future lateral resolutions near 2nm appear possible [33].

C. Contrast Mechnisms

The intensity changes with photon energy or x-ray polarization discussed in the previous section naturally lend themselves as contrast mechanisms for scanning and imaging x-ray microscopy. For example, if the photon energy is tuned to 707eV, the L_3 resonance of Fe metal (see Figure 2), the measured signal from the sample will emphasize Fe over other elements in the sample. If we change the polarization from linear to circular Fe regions in the sample will be emphasized whose magnetization direction is parallel to the photon spin (see Figure 4). It is not necessary in many cases to change the photon spin in XMCD microscopy since the contrast is large and can be enhanced by combining images recorded at the L_3 and L_2 edges.

For antiferromagnets the photon energy of the linearly polarized light is tuned to a particular multiplet peak, e.g. one of the L_2-edge peaks in Fig. 5. Domains with an orientation of the magnetic axis parallel to $\vec{E}$ will then show a different intensitiy than those with the axis perpendicular to $\vec{E}$. Again the contrast can be enhanced by combining images taken at different photon (multiplet) energies. In addition to the spectroscopic contrast other basic contrast mechanisms exist. In X-PEEM the electron yield from different sample areas is also determined by the local work function and topology. In scanning transmission x-ray microscopy additional contrast arises from differences in the x-ray absorption coefficient at non-resonant photon energies caused by compositional changes or thickness variations of the sample.

D. Surface versus Bulk Sensitivity

X-ray transmission microscopy samples the average absorption along the photon path. In the soft x-ray region the $1/e$ absorption length is typically of the order 100nm but it varies greatly near the absorption edges due to resonance effects. This is illustrated in Figure 8 for the metals Fe, Co and Ni. At the L_3 edges the x-ray absorption length is only about 15-20nm [34]. In order to avoid saturation effects, for quantitative measurements the sample should not be thicker than about 2-3 times the x-ray absorption length [35]. For practical sample thicknesses of 50nm or more, surface effects are typically negligible and x-ray transmission microscopy is therefore bulk sensitive.

In contrast, the X-PEEM signal originates closer to the sample surface. The sampling depth is determined by the cascading process of the scattered Auger electrons created after core excitation. The $1/e$ sampling depth is about 1.7nm for Fe and 2.5nm for Co and Ni [34]. Figure 9 illustrates the practical sampling depth for several multilayer samples. For example, it is seen that the signal from a $Ni_{60}Fe_{40}$ layer buried under a 4nm Co plus 1nm Ru layer can still be seen. The figure also shows results for a Co layer buried under Ag or Rh capping layers. The escape depth, which is largely determined by scattering processes from filled to empty d states and scales inversely with the number of d holes [36], is longer in Ag ($\sim$ 4.1nm) than in Rh ($\sim$ 2.5nm). The Co signal is still clearly visible through a 10nm Ag layer. As a rule of thumb one can still "see" layers that are buried as deep as 3 times the $1/e$ sampling depth.

IV. CONCLUSIONS

XMCD and XMLD spectro-microscopies are shown to offer many useful and important capabilities for the study of ferromagnets, ferrimagnets and antiferromagnets. In comparison to the many other magnetic microscopy techniques like Kerr microscopy, spin-polarized LEEM, scanning electron microscopy with polarization analysis (SEMPA), Lorentz microscopy and magnetic force microscopy (MFM), to name a few, the x-ray techniques offer some unique advantages such as elemental and chemical contrast, variable depth sensitivity and the ability to study antiferromagnets.

Relative to the other techniques, however, XMCD and XMLD microscopies are still in an infancy state. Although many examples of "test patterns" have been published [4,5,37–41] the challenge clearly lies in impacting the field of magnetic phenomena and materials. One may identify three important length scales for magnetic imaging which consecutively decrease by factors of 100. The first one is about 1μm, set by the size of lithographically fabricated magnetic cells such as in spin valve heads or magnetic memory cells. The second one is about 10nm, corresponding to the crystallographic grain size of typical magnetic materials. The final one is 0.1nm, the atomic size. Impact can occur on all three length scales, but even for the largest length scale one would like to have

a spacial resolution of 0.1μm. Todate only the best X-PEEM instruments have therefore sufficient resolution. Advances in instrumentation remain a challenge.

Acknowledgements This research was supported by the Laboratory Technology Research Partnership Program, Office of Energy Research, US Department of Energy under a CRADA (Cooperative Research and Development Agreement) between Lawrence Berkeley National Laboratory and IBM, Almaden, and by the Office of Energy Research, Office of Basic Energy Sciences, of the U.S. Department of Energy, under contract No. DE-AC03-76SF00098.

FIG. 1. Illustration of various applications of magnetic devices in computers. In magnetic memory cells the 1 and 0 bits correspond to different magnetization directions in the red layer. The bit is written by the magnetic field surrounding the current in a write line. The bit is read by a current flowing through the cell, either a spin valve [3] or tunnel valve [42]. Through a change in resistance the current senses whether the magnetization directions in the blue and red ferromagnetic layers are aligned parallel or antiparallel. The most advanced magnetic read heads are spin valves, consisting of two ferromagnetic layers (red and blue) separated by a non-magnetic layer (yellow). The blue layer is pinned by exchange coupling to an antiferromagnet shown in green. The spin valve senses, through the giant magnetoresistive effect, the direction of the magnetic flux emerging from the magnetic domains of a recording disk which rotates underneath. The magnetic flux rotates the magnetization direction in the red layer relative to the fixed direction in the blue layer. The flux density is highest at the transition regions between the magnetic bits and depends on the width of the transition regions. The width is kept small by using a granular magnetic alloy in which the grains are partially decoupled from each other by non-magnetic skins containing elements like B or Ta.

FIG. 2. a) Principles of x-ray absorption spectroscopy, using a one-electron model for the case of L-edge absorption in a d-band transition metal [13]. In the x-ray absorption process an electron is excited from the core shell to empty valence states. This results in pronounced resonances at the absorption thresholds as illustrated in b) for the $2p_{3/2} \rightarrow 3d$ (L_3-edge) and $2p_{1/2} \rightarrow 3d$ (L_2-edge) excitations in Fe and Co and the $3d_{5/2} \rightarrow 4f$ (M_5-edge) and $3d_{3/2} \rightarrow 4f$ (M_4-edge) excitations in Tb. Here the x-ray absorption spectrum for a $Tb_{24.5}Fe_{70.5}Co_{5.0}$ alloy is shown, recorded by means of total electron yield detection. The L-edge resonances for Fe and Co and the M-edge resonances for Tb are indicated in different colors. c) Fine structure of the Fe L_3 resonance in a partially oxidized Fe thin film, illustrating the chemical specificity of x-ray absorption spectroscopy.

FIG. 3. Origin of polarized synchrotron radiation from a bending magnet source. If radiation in the plane of the electron orbit is selected by a suitable aperture, linearly polarized radiation is obtained as illustrated on the right side of the Figure. By selecting radiation below or above the orbit plane right or left handed circularly polarized radiation is obtained, as explained in the text. Linear polarization can be described by a biaxial vector and handed circular polarization by a vector, the photon spin.

FIG. 4. Principles of x-ray magnetic circular dichroism spectroscopy, illustrated for the case of L-edge absorption in a d-band transition metal. In a magnetic metal the d valence band is split into spin-up and spin-down states with different occupation. Absorption of right (left) circularly polarized light mainly excites spin-up (spin-down) photoelectrons. Since spin flips are forbidden in x-ray absorption the measured resonance intensity directly reflects the number of empty d band states of a given spin. In XMCD spectroscopy it is equivalent whether the photon polarization is changed and the magnetization direction is kept fixed or whether the magnetization direction is changed and the photon helicity is fixed. The corresponding XMCD spectra for Fe metal [43] are shown on the right for three different orientations of the magnetization directions relative to the fixed photon spin (right circular polarization).

FIG. 5. Principles of x-ray magnetic linear dichroism spectroscopy, illustrated for NiO. In the x-ray absorption process core electrons are excited from the $2p$ shell to empty d states. The x-ray absorption spectrum of NiO exhibits additional fine structure at the L_3 and L_2 absorption edges arising from final state multiplet coupling of the $2p$ core hole with the d valence hole ($2p^5 3d^9$ configuration [44]). Both edges exhibit a linear dichroism effect for alignment of the $\vec{E}$ vector parallel versus perpendicular to the magnetic axis. The spectra were recorded by surface sensitive electron yield for a 45nm thick NiO(100) film grown on MgO(100). Near the surface the magnetic axis is preferentially perpendicular to the surface. The green curve corresponds to $\vec{E}$ perpendicular to the surface and the red curve for $\vec{E}$ parallel to the surface.

FIG. 6. Principles of scanning x-ray microscopy and x-ray photoelectron microscopy. In the scanning mode a small x-ray spot is formed by a suitable x-ray optic, e.g. a zone plate as shown, and the sample is scanned relative to the x-ray focal spot. The spatial resolution is determined by the spot size. The intensity of the transmitted x-rays or the fluorescence or electron yield from the sample are detected as a function of the sample position and thus determine the contrast in the image. In x-ray photoelectron microscopy the x-rays are only moderately focused in order to match the field of view of an electron microscope. Electrons emitted from the sample are projected with magnification onto a phosphor screen and the image can be viewed in real time at video rates. The spatial resolution is determined by the electron optics within the microscope, the size of the aperture and the operation voltage.

FIG. 7. a) Schematic illustration of the photoelectron energy distribution from the sample after x-ray excitation. The photoemission spectrum is dominated by the low energy scattered electrons (inelastic tail). The aperture in the backfocal plane of the PEEM shown in Fig. 6 leads to an electron energy filtering effect so that only the electron intensity shown in red is transmitted.

FIG. 8. X-ray absorption length ($1/e$ attenuation) for Fe, Co and Ni in the L-edge region [34]. The absorption lengths in the pre-edge regions (not shown) are about 600nm.

FIG. 9. Illustration of the effective secondary electron sampling depth in various metal multilayers as discussed in the text.

---

[1] For a review see IBM J. Res. Develop. **42**, 3-103 (1998).
[2] J. M. Daughton, Thin Solid Films **216**, 162 (1992).
[3] D. Tang *et al.*, IEEE Trans. Mag. **31**, 3206 (1995).
[4] J. Stöhr *et al.*, Science **259**, 658 (1993).
[5] C. M. Schneider *et al.*, Appl. Phys. Lett. **63**, 2432 (1993).
[6] B. T. Thole, G. van der Laan, and G. A. Sawatzky, Phys. Rev. Lett. **55**, 2086 (1985).
[7] G. van der Laan *et al.*, Phys. Rev. B **34**, 6529 (1986).
[8] G. van der Laan and B. T. Thole, Phys. Rev. B **43**, 13401 (1991).
[9] P. Kuiper *et al.*, Phys. Rev. Lett. **70**, 1549 (1993).
[10] D. Alders *et al.*, Europhys. Lett. **32**, 259 (1995).
[11] Sometimes the term spectro-microscopy is used only for true imaging techniques such as PEEM, while the term micro-spectroscopy is used for scanning techniques.
[12] The handedness of circularly polarized light is not uniquely defined. We follow Feynman and the convention used in particle physics. See R. P. Feynman and R. B. Leighton and M. Sands, *The Feynman Lectures on Physics, Vol. I, Part 2*, Addison-Wesley, Reading (1964).
[13] J. Stöhr and Y. Wu, in *New Directions in Research with Third-Generation Soft X-Ray Synchrotron Radiation Sources*, edited by A. S. Schlachter and F. J. Wuilleumier (Kluwer Academic Publishers, Netherlands, 1994), p. 221.
[14] B. T. Thole, P. Carra, F. Sette, and G. van der Laan, Phys. Rev. Lett. **68**, 1943 (1992).
[15] P. Carra, B. T. Thole, M. Altarelli, and X. Wang, Phys. Rev. Lett. **70**, 694 (1993).
[16] J. Stöhr and H. König, Phys. Rev. Lett. **75**, 3748 (1995).
[17] J. Stöhr, *NEXAFS Spectroscopy*, Vol. 25 of *Springer Series in Surface Sciences* (Springer, Heidelberg, 1992).
[18] P. Carra, H. König, B. T. Thole, and M. Altarelli, Physica B **192**, 182 (1993).
[19] J. Stöhr, J. Electron Spectrosc Rel. Phenom. **75**, 253 (1995).
[20] S. Saito, M. Miura, and K. Kurosawa, J. Phys. C: Solid St. Phys. **13**, 1513 (1980).
[21] F. M. F. de Groot, J. Electron Spectrosc. Relat. Phenom. **67**, 529 (1994).
[22] J. Kirz and H. Rarback, Rev. Sci. Instrum. **56**, 1 (1985).
[23] For reviews on x-ray transmission microscopy see: J. Kirz and C. Jacobsen and M. Howells, Quarterly Rev. Biophysics **28**, 1 (1995) and G. Schmahl and D. Rudolph and B. Niemann and P. Guttmann and J. Thieme and G. Schneider Naturwissenschaften **83**, 61 (1996).
[24] G. Schneider, T. Schliebe, and H. Aschoff, J. Vacuum Sci. Technol. B **13**, 2809 (1995).
[25] B. P. Tonner and G. R. Harp, Rev. Sci. Instrum. **59**, 853 (1988).
[26] B. P. Tonner, D. Dunham, T. Droubay, and M. Pauli, J. Electron Spectrosc Rel. Phenom. **84**, 211 (1997).
[27] Instruments with energy filters have been used by Schneider et al. [5], Tonner et al. [26], Fink et al. [33], and Schmidt et al. (this volume).
[28] J. Stöhr, in *X-Ray Absorption: Principles, Applications, Techniques of EXAFS, SEXAFS and XANES*, edited by D. C. Koningsberger and R. Prins (Wiley and Sons, New York, 1988), p. 443.
[29] B. L. Henke, J. A. Smith, and D. A. Attwood, J. Appl. Phys. **48**, 1852 (1977).
[30] S. Anders, M. Scheinfein, R. Duarte, A. Cossy, T. Renner, H. Padmore and J. Diaz, LBNL report (unpublished).
[31] G. F. Rempfer, W. P. Skoczylas, and O. H. Griffith, Ultramicroscopy **36**, 196 (1991).
[32] Th. Schmidt, S. Heun, J. Slezak, J. Diaz, K. C. Prince, G. Lilienkamp and E. Bauer, article in this issue.
[33] R. Fink *et al.*, J. Electron Spectrosc Rel. Phenom. **84**, 231 (1997).
[34] R. Nakajima and J. Stöhr and I. Idzerda (to be published).
[35] P. A. Lee, P. H. Citrin, P. Eisenberger, and B. M. Kincaid, Rev. Mod. Phys. **53**, 769 (1981).
[36] H. C. Siegmann, J. Phys.: Condens. Matter **4**, 8395 (1992).
[37] B. P. Tonner *et al.*, Nucl. Instrum. Methods A **347**, 142 (1994).

[38] P. Fischer *et al.*, Z. Phys. **101**, 313 (1996).
[39] C. M. Schneider *et al.*, Synchr. Rad. News **10**, 23 (1997).
[40] C. M. Schneider, J. Mag. Mag. Mat. **175**, 160 (1997).
[41] P. Fischer *et al.*, J. Phys. D: Appl. Phys. **31**, 649 (1998).
[42] J. S. Moodera, L. R. Kinder, T. M. Wong, and R. Meservey, Phys. Rev. Lett. **74**, 3273 (1995).
[43] C. T. Chen *et al.*, Phys. Rev. Lett. **75**, 152 (1995).
[44] G. van der Laan, B. T. Thole, G. A. Sawatzky, and M. Verdaguer, Phys. Rev. B **37**, 6587 (1988).

Magnetic Technologies in Computers

Memory

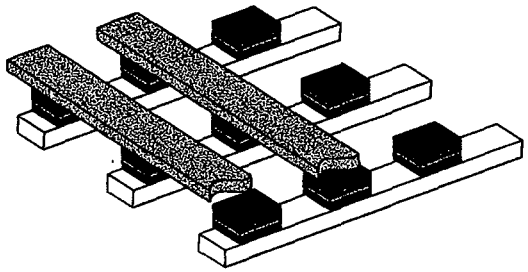

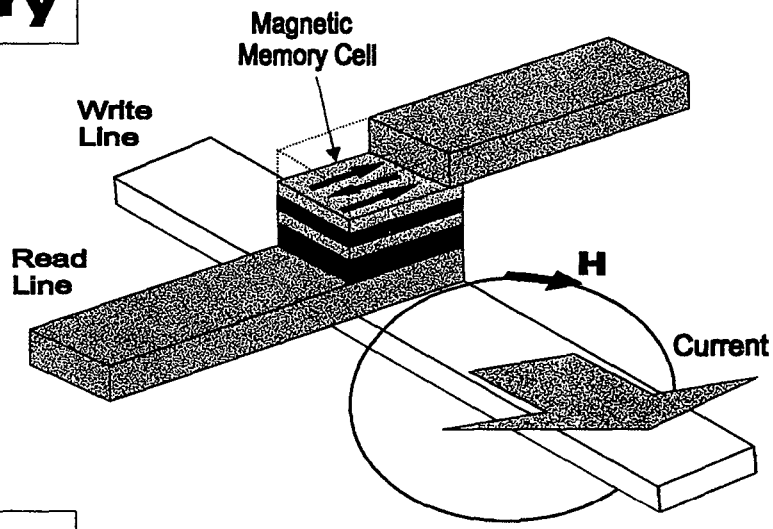

Storage

Head

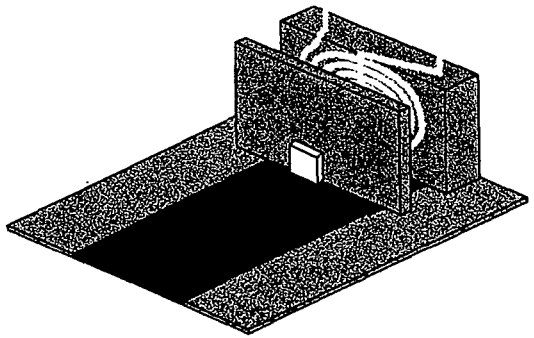

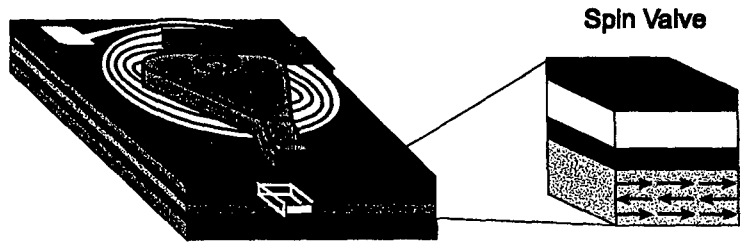

Disk

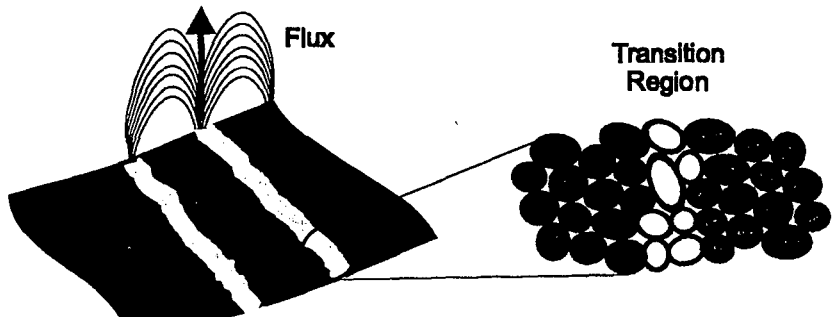

Fig. 1

X-ray Absorption Spectroscopy

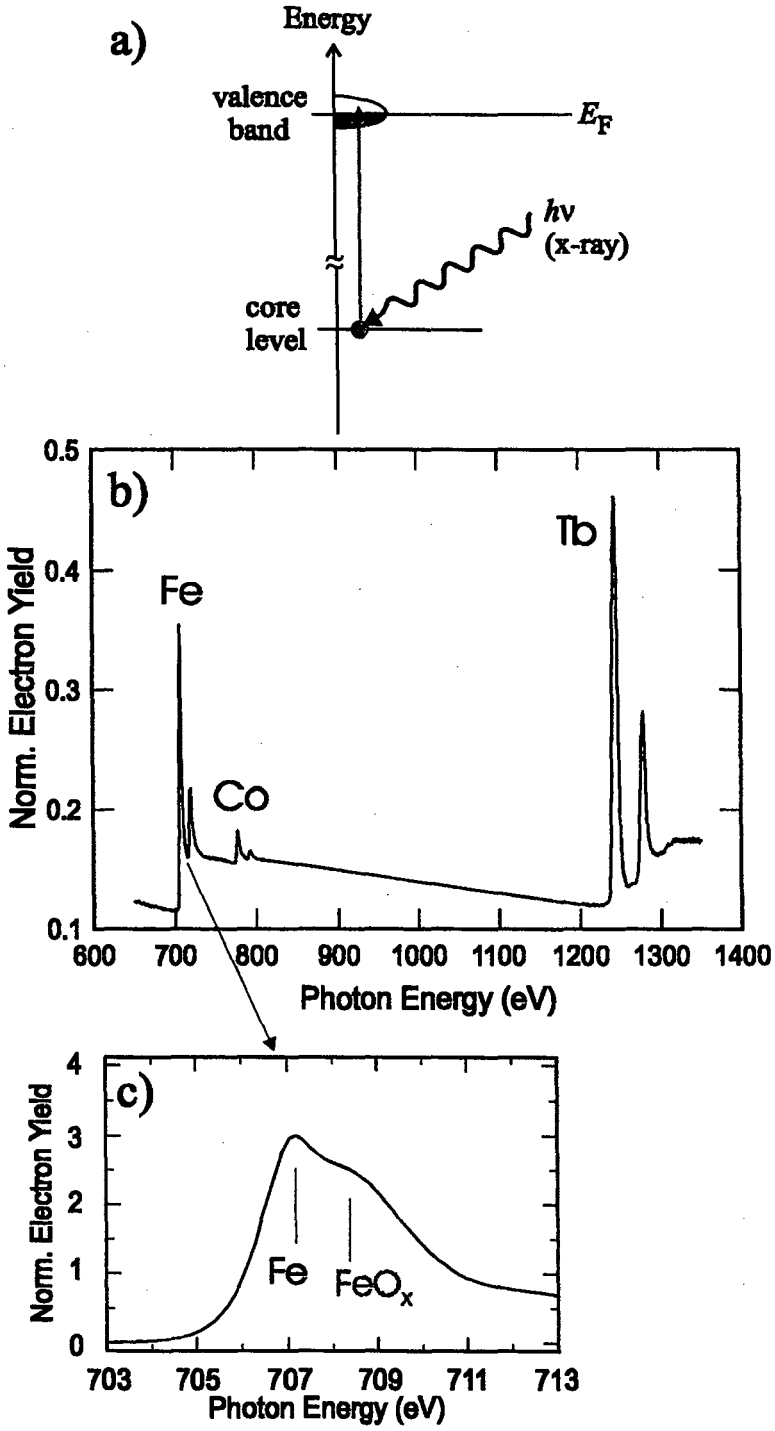

Fig. 2

XAS.cdr

Polarization of Synchrotron X-Rays

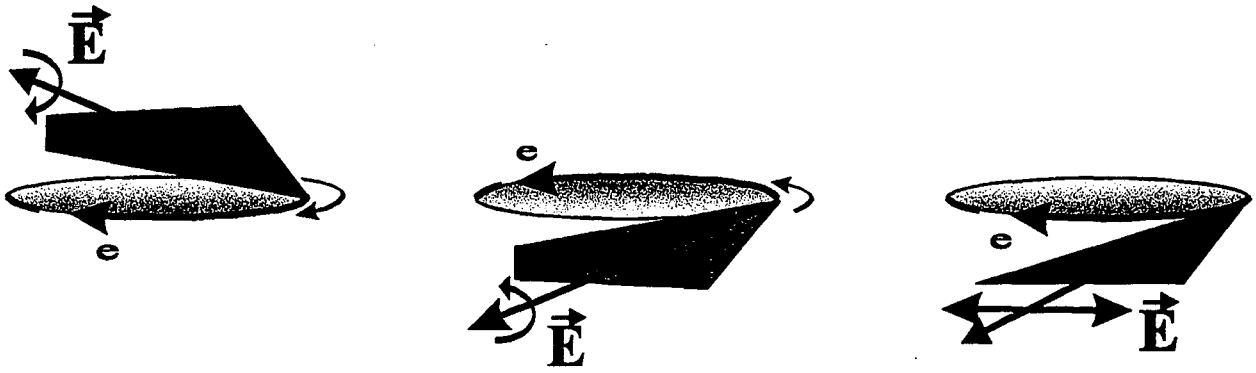

Left circular

Right circular

Linear

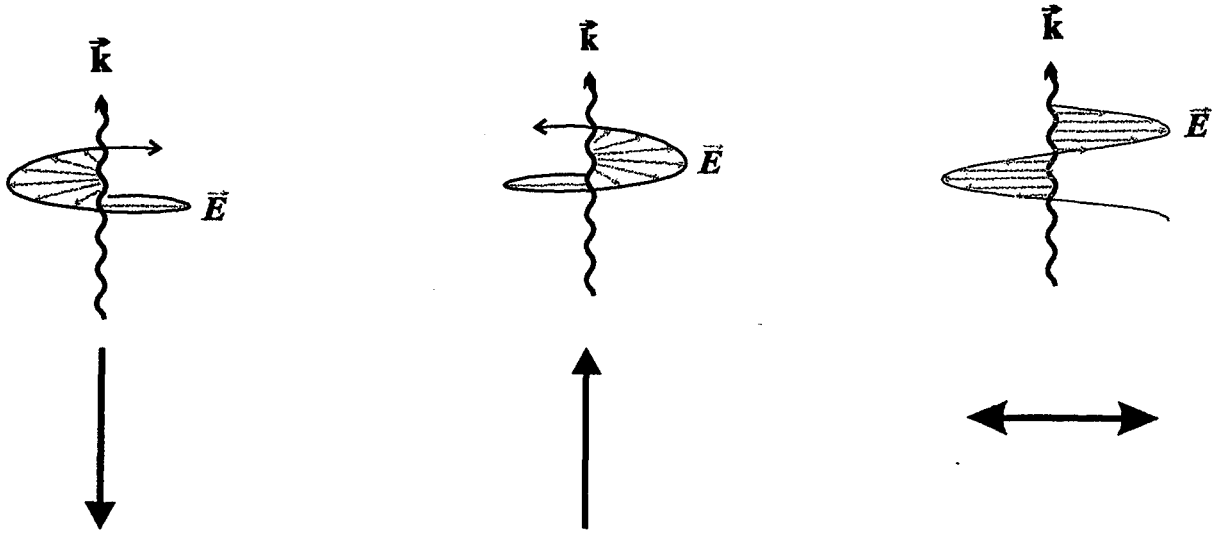

Fig. 3

Polariz.cdr

X-Ray Magnetic **Circular** Dichroism

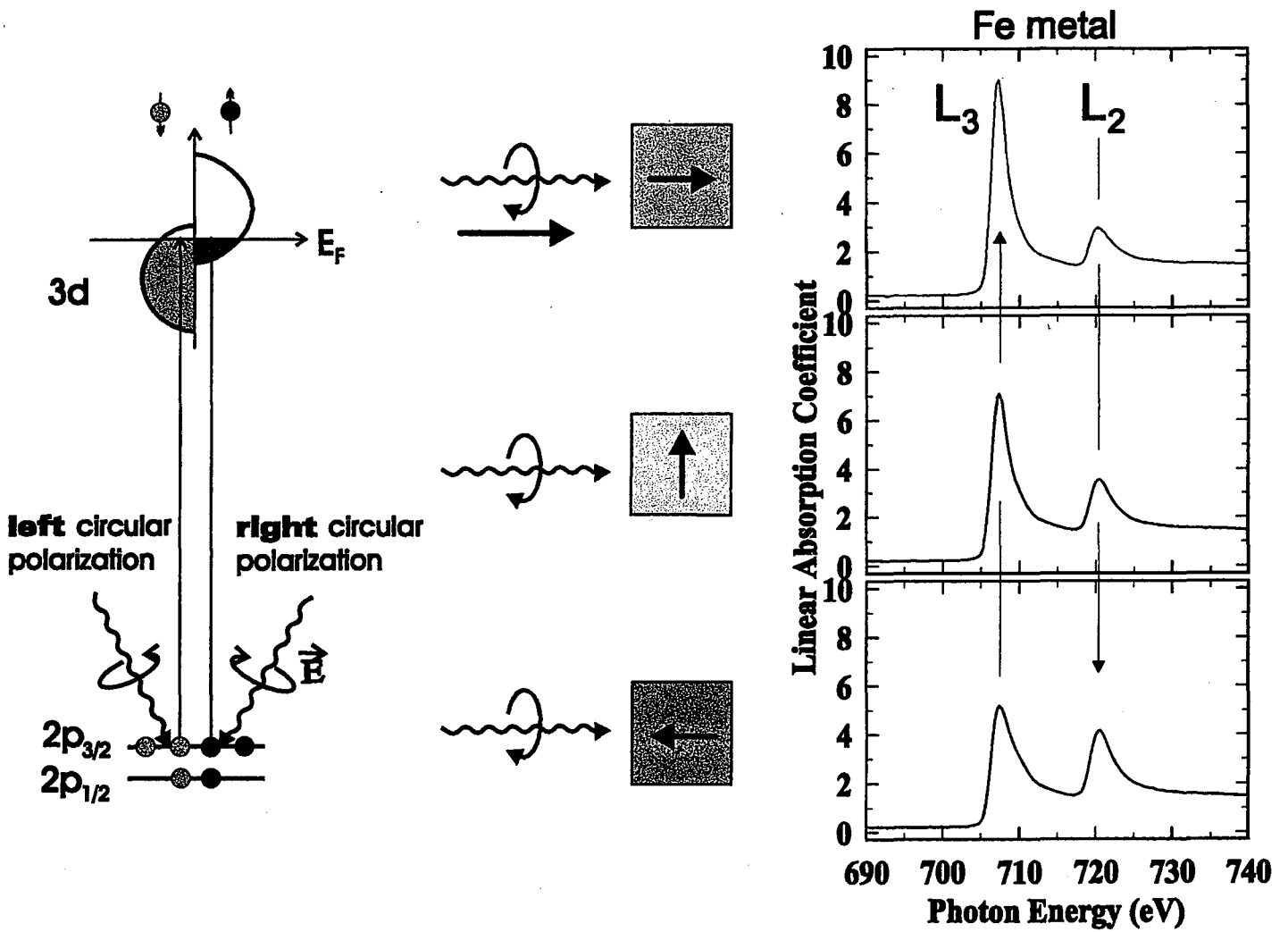

Fig. 4

xmcd.cdr

X-Ray Magnetic **Linear** Dichroism

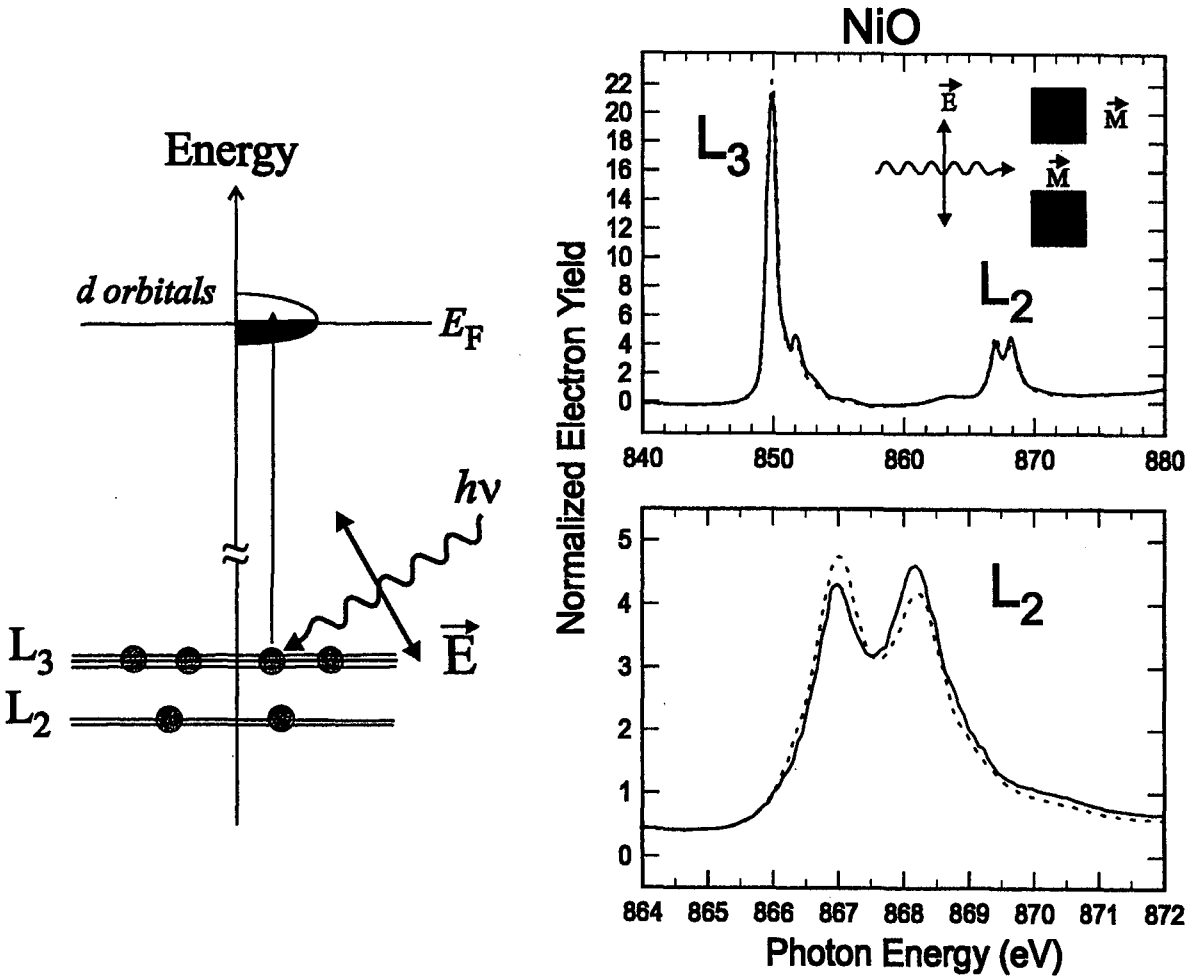

Fig. 5

xmld1.cdr

Scanning X-ray Microscopy

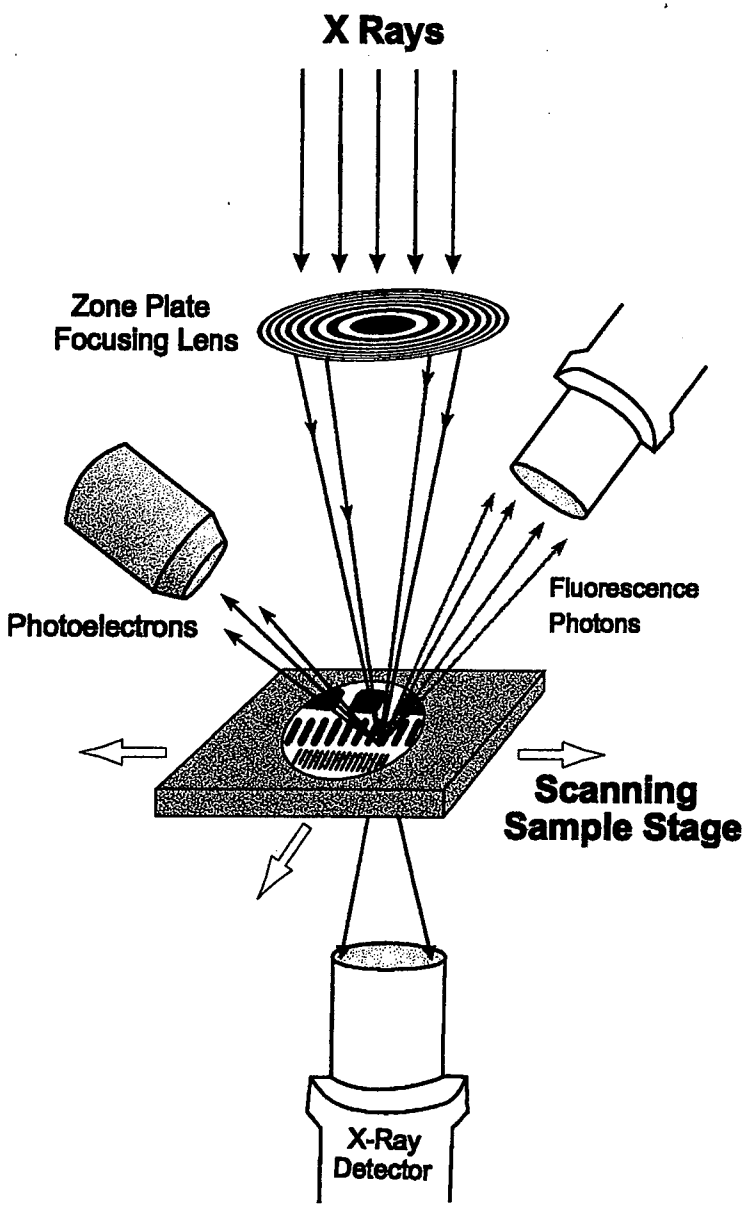

X-Ray Photoelectron Microscopy

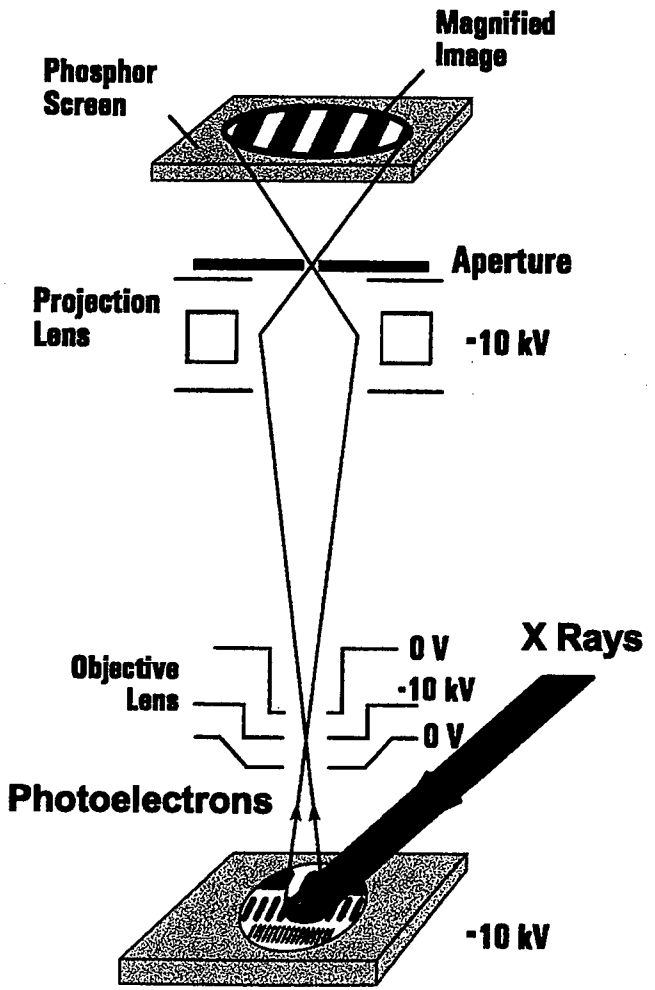

Fig. 6

stxmpeem.cdr

Distribution of Photoelectrons

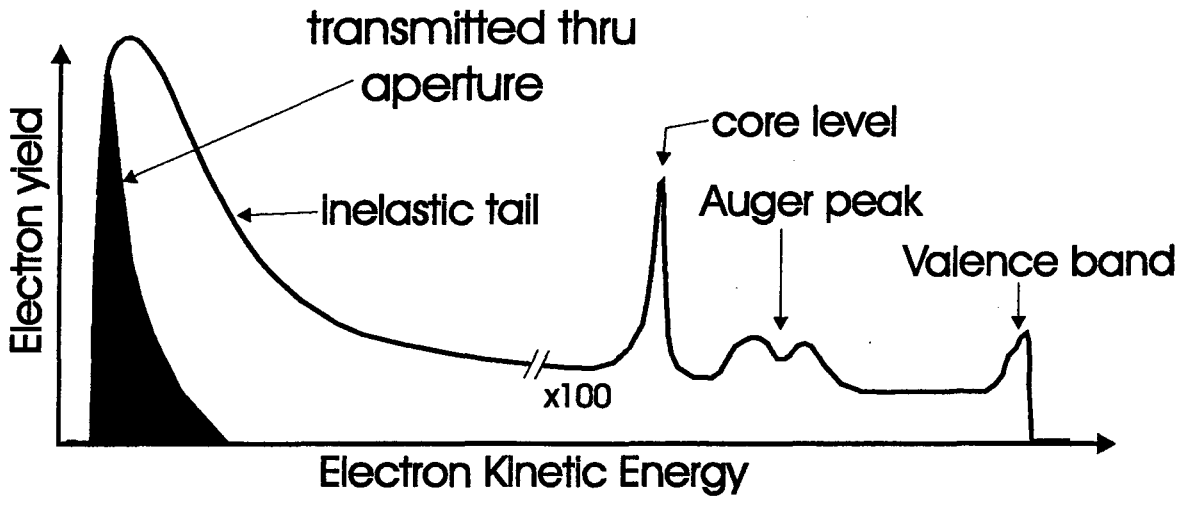

Fig. 7

aperture.cdr

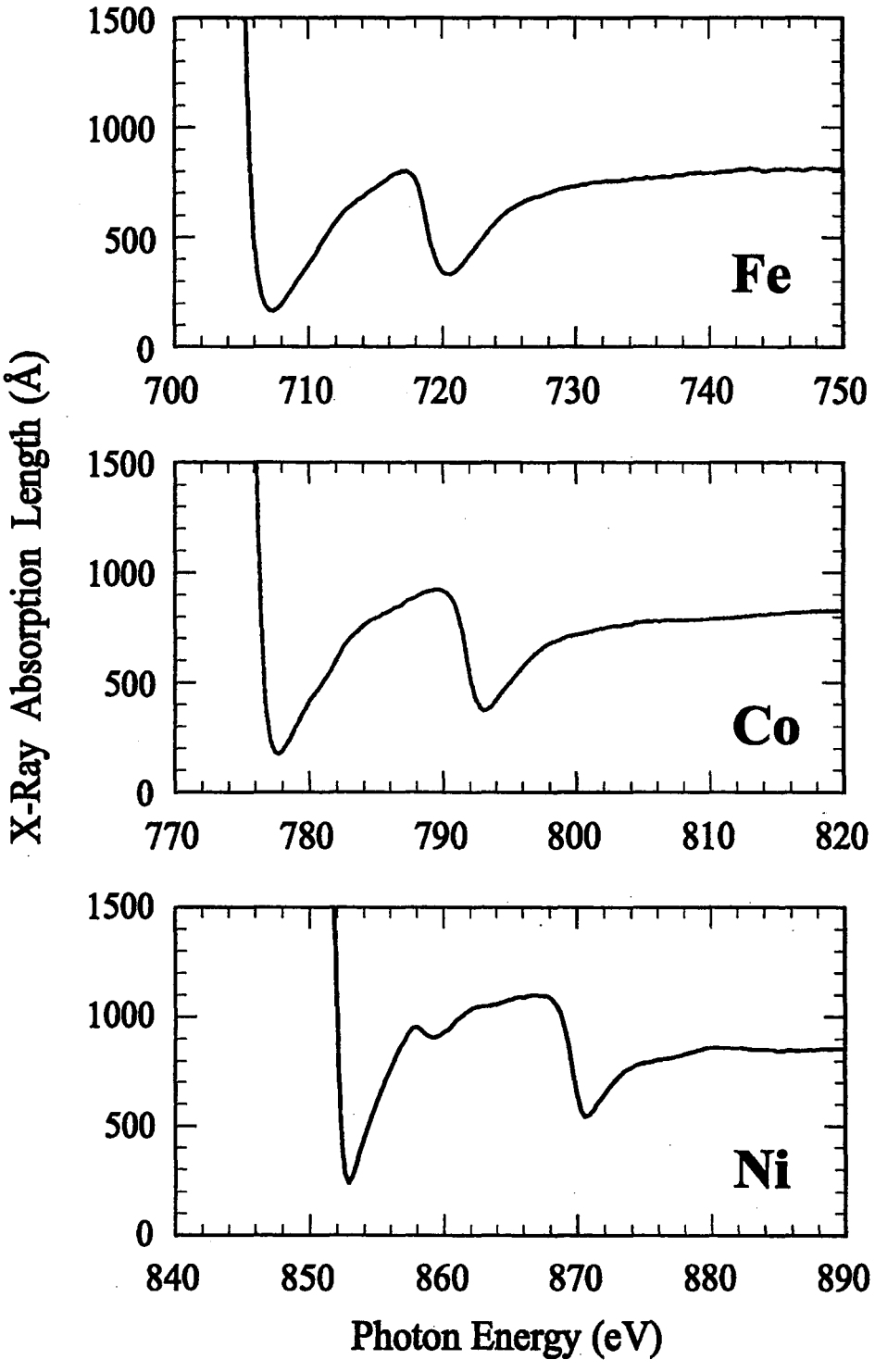

xray-dep.cdr

Fig. 8

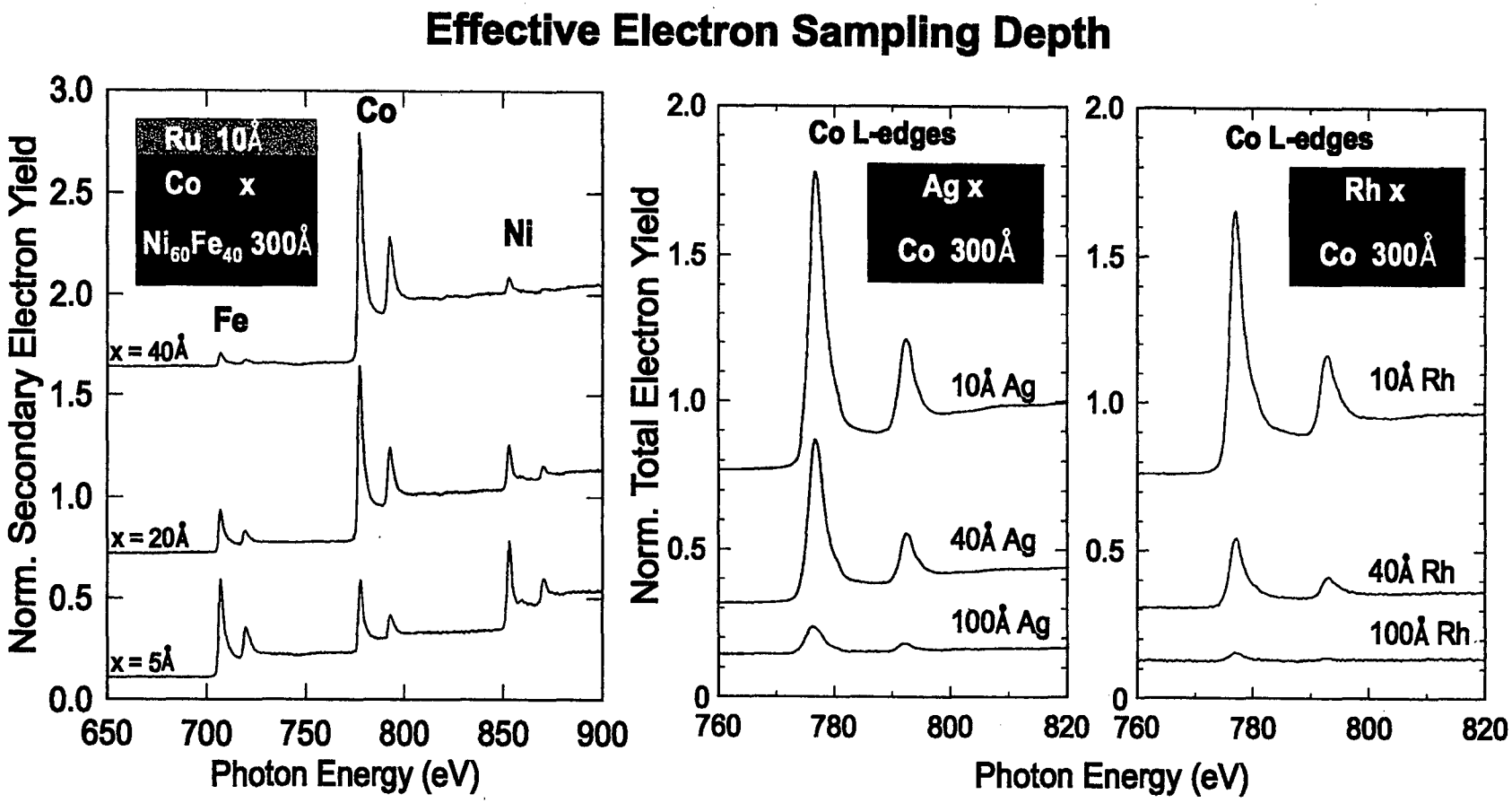
Effective Electron Sampling Depth
Norm. Secondary Electron Yield
Ru 10Å
Co x
Ni60Fe40 300Å
Co
Ni
Fe
x = 40Å
x = 20Å
x = 5Å
Photon Energy (eV)
Norm. Total Electron Yield
Co L-edges
Ag x
Co 300Å
10Å Ag
40Å Ag
100Å Ag
Co L-edges
Rh x
Co 300Å
10Å Rh
40Å Rh
100Å Rh
Photon Energy (eV)

Fig. 9

Ernest Orlando Lawrence Berkeley National Laboratory
One Cyclotron Road | Berkeley, California 94720

Prepared for the U.S. Department of Energy under Contract No. DE-AC03-76SF00098